Low Temperature Sunlight-Powered Reduction of CO_2 to CO Using a Plasmonic Au/TiO_2 Nanocatalyst

Low Temperature Sunlight-Powered Reduction of CO_2 to CO Using a Plasmonic Au/TiO_2 Nanocatalyst

Pau Martínez Molina,[a] Nicole Meulendijks,[a] Man Xu,[a, b] Marcel A. Verheijen,[c, d] Tim den Hartog,[a, e] Pascal Buskens,*[a, f] and Francesc Sastre*[a]

Sunlight-powered reduction of CO_2 to fuels and chemicals is a promising strategy to close the carbon loop and facilitate the energy transition. In this research, we demonstrate that Au nanoparticles supported on TiO_2 are an efficient plasmonic catalyst for the sunlight-powered reverse water-gas shift (rWGS) reaction. A maximum CO production rate of 429 $mmol \cdot g_{Au}^{-1} \cdot h^{-1}$ with a selectivity of 98% and an apparent quantum efficiency of 4.7% were achieved using mildly concentrated sunlight (1.44 $W \cdot cm^{-2}$ equals 14.4 sun). The CO production rate showed an exponential increase with increasing light intensity, suggesting that the process is mainly promoted by a photothermal effect. Thermal reference experiments with the same catalysts promoted CH_4 formation, dropping the CO selectivity to 70%. Thus, mildly concentrated sunlight can efficiently and selectively enhance the promotion of the rWGS reaction without using external heating.

[a] P. Martínez Molina, N. Meulendijks, Dr. M. Xu, Dr. T. den Hartog, Prof. P. Buskens, Dr. F. Sastre
The Netherlands Organisation for Applied Scientific Research (TNO)
High Tech Campus 25
5656AE Eindhoven (The Netherlands)
E-mail: pascal.buskens@tno.nl
francesc.sastrecalabuig@tno.nl
[b] Dr. M. Xu
Optics Research Group
Delft University of Technology
Lorentzweg 1 (Building 22)
2628CJ Delft (The Netherlands)
[c] Dr. M. A. Verheijen
Eurofins Materials Science
High Tech Campus 11
5656AE Eindhoven (The Netherlands)
[d] Dr. M. A. Verheijen
Department of Applied Physics
Eindhoven University of Technology
PO Box 513
5600MB Eindhoven (The Netherlands)
[e] Dr. T. den Hartog
Zuyd University of Applied Sciences
Nieuw Eyckholt 300
6400AN Heerlen (The Netherlands)
[f] Prof. P. Buskens
Institute for Materials Research
Design and Synthesis of Inorganic Materials (DESINe)
Hasselt University
Agoralaan Building D
B-3590 Diepenbeek (Belgium)

Supporting information for this article is available on the WWW under https://doi.org/10.1002/cctc.202100699

Reduction of CO_2 to fuels and chemicals is an important technology that will contribute to achieving a carbon neutral society.[1] CO_2 can be considered as a non-toxic, cheap and abundant feedstock to make synthetic fuels and chemicals. However, its activation requires high amounts of energy. Several technologies to convert CO_2 into fuels and chemicals have emerged in the last decades, such as biochemical, electrochemical, thermochemical, plasma chemical and photochemical.[2–6] Photocatalysis aims to directly harvest (sun) light and transfer its energy to convert CO_2 into fuels and chemicals.[7–11] Different products can be targeted through (sun) light-powered CO_2 hydrogenation, with methane (CH_4) and carbon monoxide (CO) as the main target products.[12–18] Recently, plasmonic hydrogenation of CO_2 to CH_4 [Sabatier reaction, Eq. (1)] has been reported with high production rates using Ru and Ni based catalysts at low catalyst bed temperatures.[18–32] CO is an interesting product to target due to the great potential it offers as a building block to synthesize long chain hydrocarbons through the well-established Fischer-Tropsch synthesis (FTS). CO_2 is hydrogenated to CO via the reverse water-gas shift (rWGS) reaction [Eq. (2)]. The combination of the rWGS reaction and the FTS constitutes a two-step process which has potential to become a green technology for the production of synthetic fuels with large demand using CO_2 as a feedstock.[33–36]

$$CO_2 + 4H_2 \rightarrow CH_4 + 2H_2O \ \Delta H_{298K} = -165.0 \text{ kJ } mol^{-1} \quad (1)$$

$$CO_2 + H_2 \rightleftharpoons CO + H_2O \ \Delta H_{298K} = 41.2 \text{ kJ } mol^{-1} \quad (2)$$

The rWGS reaction is endothermic and limited by equilibrium. With thermocatalysis, at temperatures below 600 °C, CH_4 is the main formed product through an exothermic reaction which is the main competing process of the rWGS reaction.[36–37] Traditionally, to increase the CO selectivity to around 80%, temperatures above 800 °C are required.[37] This can lead to particle sintering, coke formation and a fast catalyst deactivation. Cu, Rh and Pt based catalysts have shown the highest activities of all the high-temperature resistant catalysts reported.[38–40] As an alternative, photocatalysis aims to use photoactive materials which can harvest sunlight to either increase their (local) temperature or excite a charge carrier in order to catalyze the reaction either photothermally or photochemically.[41–45] Conventionally, semiconductor materials have been used as photocatalysts but they can only harvest light in the UV region, which corresponds roughly to 4% of the

solar spectrum. To improve the light harvesting at different frequencies, metallic nanoparticles (NPs) which display plasmonic behavior under light irradiation are a promising upgrade to these materials. Determining the role of the different mechanisms involved in the process and differentiating between the thermal and non-thermal contribution to the overall catalytic performance is of great interest from both scientific and application perspective.[43–58] Here, we contribute to identify the various physical mechanisms involved in the plasmonic sunlight-powered Au/TiO_2 catalyzed rWGS reaction.

Only few groups have reported on the rWGS reaction under light irradiation. Noble metal catalysts based on Au and Ag have been reported to have the highest activities. Huber *et al.* studied the performance of Au NPs supported on different metal oxides at 400°C under visible light irradiation (5216 $W\,m^{-2}$), reporting an apparent quantum efficiency with Au/TiO_2 of 5% and a CO production rate of 2663 $\mu mol\cdot g_{cat}^{-1}\cdot min^{-1}$.[59] Several catalysts based on Au and Ag NPs supported on TiO_2 were studied by Tahir *et al.*, unravelling the potential of different TiO_2 morphologies and the use of bimetallic catalysts. They investigated Au/TiO_2 nanostructures, with maximum activity of 4144 $\mu mol\cdot g_{cat}^{-1}\cdot h$ under 150 $mW\,cm^{-2}$ light intensity irradiation.[60–62] Some earth-abundant metals can promote the rWGS reaction but with lower CO productions rates.[63–64] Ouyang *et al.* studied several group VIII metals supported on Al_2O_3, demonstrating the potential of Fe-based plasmonic catalysts, which promoted the rWGS reaction with an activity of 19.2 $mmol\cdot g^{-1}\cdot h^{-1}$ under irradiation of a 300 W Xe lamp.[63] The group of Halas reported that Al/Cu_2O was active for the CO_2 reduction to CO getting a production rate of 10 $\mu mol\cdot cm^{-2}\cdot s^{-1}$ under highly concentrated laser light irradiation (10 $W\cdot cm^{-2}$) without additional external heating.[64]

In this study, we report a catalyst based on Au NPs supported on anatase TiO_2 (Au/TiO_2) which selectively promotes the formation of CO from CO_2 and H_2 with the sole energy input of slightly concentrated sunlight. We attribute the excellent results to the great sunlight-harvesting ability of this catalyst, caused by the localized surface plasmon resonance (LSPR) of the Au NPs, which capture a large portion of the solar spectrum. Based on combined experimental and theoretical analyses, we propose that the mechanism promoting the reaction involves a synergistic contribution of photothermal and photochemical processes. The main contribution to the activity results from the Au NPs acting as nano-heaters to enhance the reaction photothermally, while charge transfer processes are crucial to desorb the formed H_2O and CO from the Au/TiO_2 catalyst surface. We see the possibility to operate at low catalyst bed temperature and almost ambient reactor temperature ($<30\,°C$) as a unique feature for the scalability of the process into an industrial application, which can efficiently reduce CO_2 to CO with a selectivity of 98% and a quantum efficiency of 4.7%.

The Au/TiO_2 catalyst was prepared via a deposition-precipitation method (see Experimental Section). The Au content was determined by Inductively Coupled Plasma-Atomic Emission Spectroscopy (ICP-AES) obtaining a value of 3.12 wt% Au. The particle size distribution was determined based on images from High-Angle Annular Dark Field Scanning Transmission Electron Microscopy (HAADF-STEM). A representative image is shown in Figure 1a. The Au particle size distribution follows a lognormal distribution, with an average particle size of 1.6 nm (Insert Figure 1a). Figure 1b displays a representative, crystalline Au NP, present on the surface of a TiO_2 crystal. The interplanar distance in the Au NP is 2.37 Å ± 0.02 Å, corresponding to the (111) spacing. The (111) lattice planes are perfectly aligned with the (101) TiO_2 planes. The diffuse reflectance spectra (UV-Vis) were measured for the TiO_2 and Au/TiO_2 particles and are presented in Figure 1c.

As it can be observed, the TiO_2 only absorbs in the UV region (<400 nm) while the Au/TiO_2 has a broad band absorption in the UV and visible region due to the plasmonic nature of the Au NPs. The maximum absorbance was observed in the range between 500 and 600 nm, corresponding to the LSPR frequency of Au nanospheres. The X-ray diffraction (XRD) pattern confirms the main presence of the TiO_2 anatase based on the positions of the diffraction peaks (Figure 1d). The characteristic diffraction peaks of Au were detected at 36.9° and 44.6° and 62.7°.

The sunlight-powered CO_2 reduction experiments with H_2 were performed in a custom designed batch photoreactor system (Figure S1), equipped with a quartz window through which artificial sunlight was irradiated on the catalyst. The reactor was heated via electric heaters to perform comparative thermocatalytic experiments (dark tests). The photoreactor was loaded with 200 mg of the catalyst and filled until a total pressure of 3.5 bar with a mixture of CO_2:H_2:N_2, with a volumetric ratio of 2:2:1. N_2 was used as internal standard (see Experimental Section). The light source was a solar simulator (Newport Sol3 A) equipped with an AM1.5 filter and a light concentrator that can reach a maximum intensity of 14.4 sun. The catalyst bed temperature was measured through a thermocouple placed in contact with the bottom side of the catalyst bed to avoid direct exposure of the thermocouple to light. This temperature does not correspond to the catalyst top surface temperature which will be notably higher as discussed in the following sections. The reactor temperature was measured at the top and bottom of the reactor. Time zero was considered when the light was switched on. For the dark experiments, the reactor was heated from the bottom and laterals. Prior to the experiments, the system was allowed to reach thermal equilibrium at the desired temperature and then filled with the reactants.

The CO evolution on Au/TiO_2 was studied under 14.4 sun for 3 hours without an external heat source, with an initial reactor temperature of 20 °C. The CO production is shown in Figure 2a.When the light was switched on, the catalyst bed temperature reached 135 °C rapidly (Figure 2b, black line). In contrast, the reactor temperature remained stable between 20 °C and 30 °C for the 3 h of reaction time (Figure 2b, blue line). The main detected product was CO, with a selectivity of 98.2% throughout the 3 h reaction period. The initial CO production rate was 429.2 $mmol\cdot g_{Au}^{-1}\cdot h^{-1}$ (13.4 $mmol\cdot g_{cat}^{-1}\cdot h^{-1}$) after 15 min and the only other detected product was CH_4. The apparent quantum efficiency was 4.7% (Equation S1), leading to a final CO concentration in the reactor

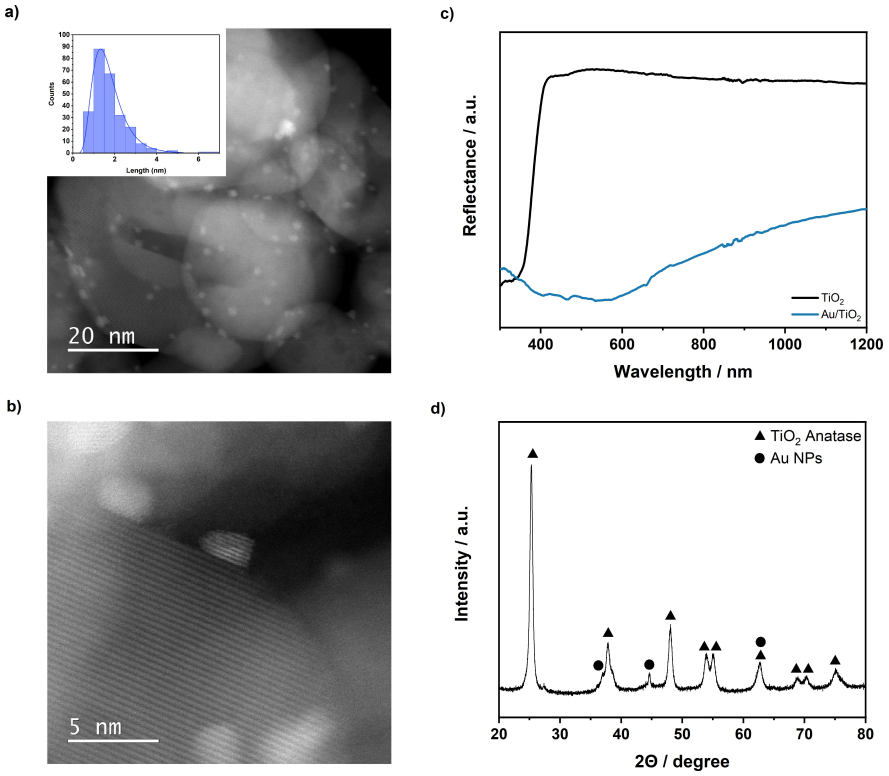

Figure 1. a) Representative image with particle size distribution histogram for Au and **b)** high resolution image from the HAADF-STEM of the 3.12 wt% Au/TiO_2 catalyst, **c)** Diffuse reflectance UV-Vis-NIR spectra for TiO_2 (black) and Au/TiO_2 (blue), **d)** XRD pattern of the 3.12 wt% Au/TiO_2 sample

of 4.9%. This is a remarkably high efficiency considering that CO production is selectively promoted at high temperatures, and in this case only solar light was irradiated onto the system without any external source of heat. Control experiments showed that no products were detected when Au was not present on the TiO_2 support achieving a catalyst bed temperature of 55 °C (Figure S2). In order to confirm that CO_2 was the sole carbon source, an experiment with no CO_2 presence in the reactor was performed under light irradiation (14.4 sun), in which no products were detected.

To distinguish between photothermal and photochemical processes, we studied the relationship between light intensity and CO production rate. Figure 3a shows that the CO production rate under artificial sunlight illumination (black squares) follows an exponential curve with increasing light intensity between 6 and 14.4 sun. This suggests that the process is mainly driven by photothermal processes, as reported by Baldi *et al.*[47] The Au NPs harvest sunlight through the LSPR mechanism to excite charges, and a large part of these decay thermally, efficiently heating the local spots at which the reaction takes place. Through this, the plasmonic particles promote the rWGS reaction via a photothermal effect. However, this does not completely rule out the possibility of an additional influence from photochemical processes. With the temperature obtained via a thermocouple in direct contact with the bottom of the catalyst bed (Figure S1, S2b), we calculated an apparent activation energy of 29 $kJ \cdot mol^{-1}$ for the light-powered reaction using Arrhenius equation (Eq. S2). This is similar to the apparent activation energy reported for the Au/TiO_2 catalyzed, light-powered rWGS reaction reported by Huber and coworkers (35 $kJ \cdot mol^{-1}$).[59] Figure S3a shows the CO evolution during the 3 h reactions at all the different light intensities. It can be observed that the total equilibrium concentration of CO was lower at lower intensities, which was expected due to the lower local temperatures. The relation between the bulk catalyst bed temperature and light intensity followed a linear trend, as seen in Figure S3b.

In order to differentiate between the role of the Au and the TiO_2, a set of experiments without UV light was performed. The solar spectrum (AM1.5) contains around 4% of UV light that can largely contribute to the photocatalytic activity. In this set of experiments, a 395 nm long pass filter was added to the solar simulator. This filter blocked the UV light ($<$395 nm, Figure S4), which does not overlap with the plasmonic band of the Au NPs and can only be absorbed by the TiO_2. We corrected for the loss in light intensity caused by using the UV long pass filter (Figure S5). Under these conditions, similar CO production rates were observed with and without UV light irradiation, as can be seen in the Figure 3a (blue circles). Based on this, it was concluded that Au NPs are mainly responsible for the light absorption and the promotion of the reaction. However, there must be a synergy between the Au NPs and the TiO_2 as a support, like adsorption of reactant molecules, charge transfer of the charges generated in the Au NPs to the TiO_2 semiconductor among other options, which are beyond the scope of this report.

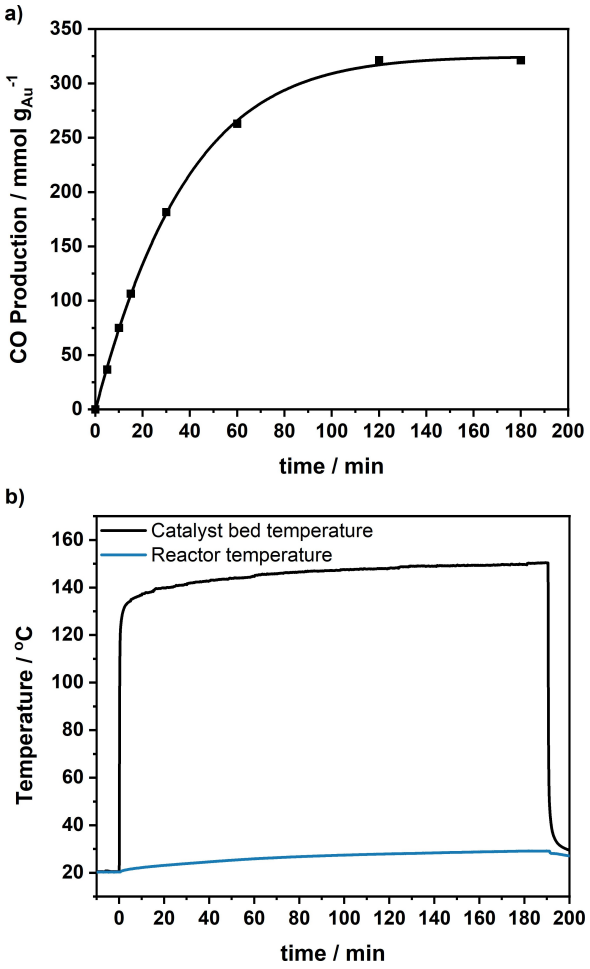

Figure 2. a) CO production vs time for the reduction of CO_2 using Au/TiO_2 photocatalyst under 14.4 sun intensity, **b)** catalyst bed temperature (black) and reactor temperature (blue) vs time. Reaction conditions: mixture of CO_2:H_2:N_2 (2:2:1) at 3.5 bar pressure (3.12 wt% Au/TiO_2, 200 mg, 14.4 sun irradiation from solar simulator (1 sun = 1 kW·m^{-2}, AM1.5))

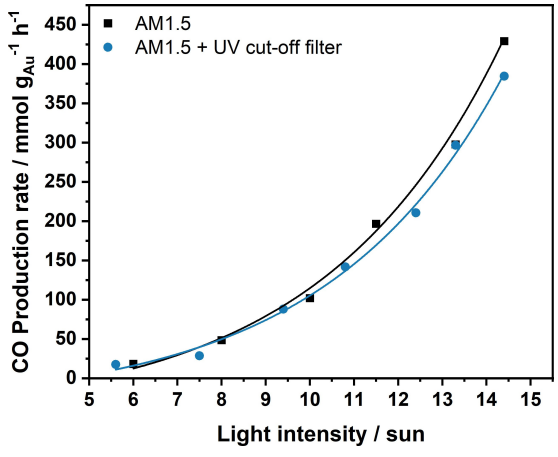

Figure 3. CO production rate vs light intensity for the reduction of CO_2 with AM1.5 filter (black squares) and AM1.5 + UV long pass filter (blue dots). The shown curves are the exponential fit for both datasets. Reaction conditions mixture of CO_2:H_2:N_2 (2:2:1) at 3.5 bar pressure (3.12 wt% Au/TiO_2, 200 mg)

The catalyst bed temperature of the tests with the UV long pass filter can be seen in Figure S3b (blue circles). These temperatures follow the same slope as for the full spectrum tests, but with a general decrease of around 20 °C. This could be caused by the elimination of the light absorption by TiO_2, which would be expected to have a thermal effect through electron-hole recombination. However, this temperature change did not have a relevant impact on the activity, therefore the measured catalyst bulk temperature proved to be an inaccurate factor to estimate activity.

To gain insight on the local Au NPs temperature of our catalyst, we performed optical modelling based on finite element method (FEM) using COMSOL Multiphysics® software.[65] The photothermal behavior of an isolated Au/TiO_2 particle was studied (Figure 4). For the modelling, we assumed that light is only absorbed by the Au NPs and not by TiO_2. This applies for the wavelength range of our simulation (400–600 nm). Because NPs are very poor light emitters, all the absorbed light is transferred into thermal energy and yields a difference between the temperature of non-illuminated and illuminated NPs (ΔT).[66] For the simulation, the light source was a monochromatic plane wave with intensity of 100 mW·cm^{-2} (1 sun). For fixed TiO_2 and Au NP sizes, the absorbed light increases as the number of Au NPs increases resulting in higher ΔT (Figure 4b). ΔT is proportional to the number of Au NPs, as the ratio of ΔT between 14 and 10 Au NPs is approximately 1.44. Additionally, the size of the carrier TiO_2 NPs affects the ΔT. The radius of the TiO_2 was varied from 5 to 20 nm, while the number of Au NPs on the TiO_2 was kept at 14. With increasing TiO_2 NP size, the temperature increase was lower. The TiO_2 carrier does not absorb light and only serves as a thermal reservoir. The larger the TiO_2 NPs, the more mass and the higher the required energy to reach the same ΔT. For 3.1 wt% Au/TiO_2, from our calculation, the temperature increase ΔT for the isolated Au/TiO_2 nano-particle was estimated to be around 10 °C under 14 sun irradiation.

Besides the isolated NP, we have estimated the photothermal response of a collective NP solid powder. Kirchhoff's law states that at thermal equilibrium, the power radiated by an object must be equal to the power absorbed for a body. We assume that our catalyst is in thermal equilibrium, and that the energy input results only from the light absorption and the energy loss is solely caused by emission which is a radiative heat transfer effect. Consequently, the Stefan Boltzmann law provides a good and easy approximation to estimate the catalyst temperature and interpret our experimental findings. For theoretical study and numerical model of the photothermal effect from nanoparticles, some publications).[67–68] from other groups can be considered. We estimate that the collective temperature only at the top surface of the Au/TiO_2 solid powder can reach as high as 300 °C under 14 sun illumination (see Figure S6). This temperature will decrease from top to bottom in the catalyst layer. In order to obtain more precise temperature profiles, the analytical model will be improved in the future work. Additionally, in the proceeding research we will explore temperature characterization method to study the T-gradient in the NPs powder. Those would be crucial to discern

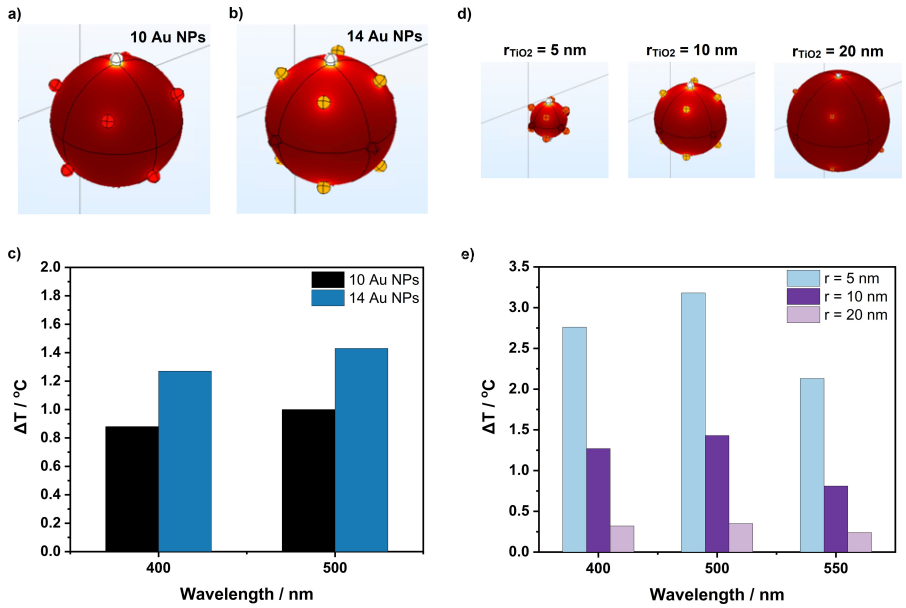

Figure 4. The temperature change of the isolated Au NP/ TiO_2 under monochromatic plane wave illumination. In **a)** geometry of 10 Au small nanospheres (2 nm) on larger TiO_2 NS, **b)** 14 Au NS on TiO_2; the color illustrates the thermal energy density, **c)** ΔT of the isolated Au NPs at wavelengths 400 nm and 500 nm, **d)** Temperature change of isolated Au NPs for varying support TiO_2 NP size (5–10–20 nm), **e)** ΔT at various irradiation wavelengths for varying support TiO_2 NP size (5–10–20 nm).

between thermal and non-thermal contributions to the catalytic process.

In order to further investigate the role of thermal versus non-thermal effects, we performed a series of dark experiments. The lowest temperature was 140 °C, as this was the measured catalyst bed temperature under 14.4 sun irradiation (Figure 2b). Under these conditions, the obtained initial CO production rate was 67 $mmol \cdot g_{Au}^{-1} \cdot h^{-1}$, 6.5 times lower than the production rate observed when light was used, underpinning that the average local temperature upon illumination was higher than that measured through the catalyst bulk bed temperature. The temporal profiles of the CO_2 hydrogenation at 140 °C and 160 °C are presented in Figure S7. At 180 °C, the CO production rate in the first 5 minutes was still lower than for the illuminated experiment (14.4 sun), as can be observed in Figure 5a. Assuming all the contribution came from photothermal processes, indicates that the local average temperature for the test under illumination was slightly above 180 °C. This is an estimation of average local temperature over the whole catalyst thickness, not to be confused with the surface temperature determined via computer modelling. Two different regimes could be differentiated in the dark reactions. Initially, the CO production rate increased similarly to the tests under irradiation. Then the CO production rate decreased largely after the first 5 minutes to completely stop after 30 min.

In contrast, the formation of CH_4 was promoted under dark conditions with an almost constant production rate for 2 h (Figure 5b), this is according what reported previously for temperatures below 600 °C.[37] while under illumination CH_4 production was mostly suppressed suggesting the thermal effect entails suppression of CH_4 as a competing reaction. For the light experiment, the CO selectivity was maintained at values around 98% over the 2 h. Instead, the CO selectivity dropped to 70% under dark conditions at 180 °C, indicating that light enhances the promotion of the rWGS reaction over the methanation reaction. This change in selectivity shows a different kinetic mechanism between the tests under illumination and the dark tests. We propose that the difference in catalyst deactivation and selectivity was due to the promotion of H_2O and CO desorption through charge transfer of plasmon generated charges, which is in linewith what has been previously reported in literature.[59,69] The favored desorption of H_2O was reflected in the lower deactivation rate, which could be caused by two different processes. First, when H_2O desorption from the reactive sites is enhanced, more reactants can be adsorbed and the reaction can continue. The second is related to the rWGS reaction being limited by the equilibrium in equation 2. When H_2O is removed from the surroundings of the reaction sites it reduces the concentration of H_2O in the vicinity of the NPs and shifts the equilibrium, promoting the CO formation following Le Châtelier's principle. In parallel, the favored desorption of CO by light is reflected in the selectivity change. As the rWGS and the Sabatier reactions often share the same mechanism, the CO desorption step is crucial to determine the selectivity of the process. If CO is desorbed, it cannot be further hydrogenated, inhibiting the CH_4 formation. This leads to significantly enhanced CO production and selectivity under light irradiation at low temperatures.

In conclusion, we have successfully demonstrated that Au/TiO_2 is able to selectively promote the rWGS reaction under slightly concentrated artificial sunlight illumination without any external heating source. The CO production rate increases

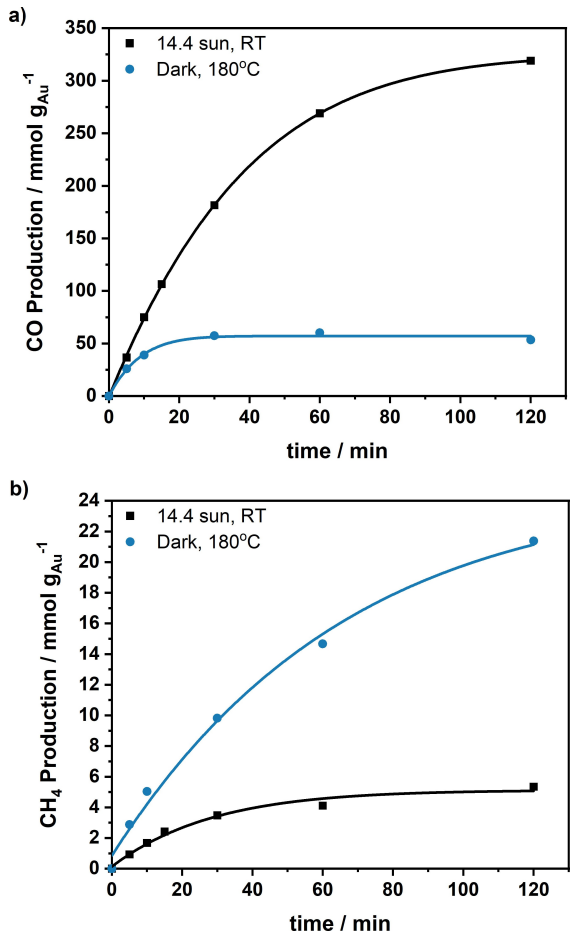

Figure 5. a) CO production vs time for the reduction of CO_2 under illumination (AM1.5,14.4 sun, black squares) and dark conditions (180 °C, blue dots) **b)** CH_4 production vs time for the reduction of CO_2 under illumination (AM1.5,14.4 sun, black squares) and dark conditions (180 °C, blue dots). Reaction conditions: mixture of CO_2:H_2:N_2 (2:2:1) at 3.5 bar pressure (3.12 wt% Au/TiO_2, 200 mg).

exponentially with the increase of the light intensity, which indicates that the reaction is mainly promoted by the thermal decay of the LSPR of the Au NPs. Although we determined that most of the activity is generated by the light absorption from the Au NPs, the TiO_2 still plays an essential role in the mechanism. The average local temperature at the Au NPs was estimated to reach around 300 °C at the surface of the catalyst bed, based on the simulated conditions through the FEM optical model. We have shown that illumination improves the catalyst activity and selectivity towards CO, possibly due to enhanced product desorption which shifts the equilibrium of the rWGS reaction towards CO and H_2O production. More specifically, light helps to efficiently promote the CO formation and suppresses the methanation reaction to achieve a CO selectivity of 98% without any external heating, reaching an AQE of 4.7% and a CO production rate of 429 mmol·g_{Au}^{-1}·h^{-1}. The high CO production and selectivity values achieved solely with sunlight and without external heating can enable the development of a sustainable process to make long chain hydrocarbon production accessible via the intermediate CO based on concentrated solar energy.

Acknowledgements

P.M., N.M., M.X., T.H., P.B. and F.S. acknowledge financial support from the European Fund for Regional Development through the cross border collaborative Interreg V program Flanders-The Netherlands (project LUMEN), co-financed by the Belgian province of Limburg and the Dutch provinces of Limburg and Noord-Brabant. M.A.V. acknowledges Solliance and the Dutch province of Noord-Brabant for funding the TEM facility. We thank Prof. dr. Wouter Marchal from the Hasselt University for the ICP analyses.

Conflict of Interest

The authors declare no conflict of interest.

Keywords: Carbon Dioxide · Reverse Water-Gas Shift · CO · solar light · Surface plasmon resonance · Photochemistry

[1] I. R. E. A. (IRENA), *Global Renewables Outlook: Energy transformation 2050*, **2020**.
[2] S. C. Roy, O. K. Varghese, M. Paulose, C. A. Grimes, *ACS Nano* **2010**, *4*, 1259–1278.
[3] Y. Zhao, W. Gao, S. Li, G. R. Williams, A. H. Mahadi, D. Ma, *Joule* **2019**, *3*, 920–937.
[4] S. Li, P. Miao, Y. Zhang, J. Wu, B. Zhang, Y. Du, X. Han, J. Sun, P. Xu, *Adv. Mater.* **2020**, e2000086.
[5] A. Senocrate, C. Battaglia, *J. Energy Storage* **2021**, *36*, 102373.
[6] A. Mustafa, B. G. Lougou, Y. Shuai, Z. Wang, H. Tan, *J. Energy Chem.* **2020**, *49*, 96–123.
[7] A. Zada, P. Muhammad, W. Ahmad, Z. Hussain, S. Ali, M. Khan, Q. Khan, M. Maqbool, *Adv. Funct. Mater.* **2019**, 1906744.
[8] A. Naldoni, F. Riboni, U. Guler, A. Boltasseva, V. M. Shalaev, A. V. Kildishev, *Nat. Photonics* **2016**, *5*, 112–133.
[9] M. L. Brongersma, N. J. Halas, P. Nordlander, *Nat. Nanotechnol.* **2015**, *10*, 25–34.
[10] F. Sastre, M. J. Muñoz-Batista, A. Kubacka, M. Fernández-García, W. A. Smith, F. Kapteijn, M. Makkee, J. Gascon, *ChemElectroChem* **2016**, *3*, 1497–1502.
[11] D. Devasia, A. J. Wilson, J. Heo, V. Mohan, P. K. Jain, *Nat. Commun.* **2021**, *12*, 2612.
[12] T. N. Do, J. Kim, *J. CO2 Util.* **2019**, *33*, 461–472.
[13] S. Alsayegh, J. R. Johnson, B. Ohs, M. Wessling, *J. Cleaner Prod.* **2019**, *208*, 1446–1458.
[14] A. Corma, H. Garcia, *J. Catal.* **2013**, *308*, 168–175.
[15] U. Ulmer, T. Dingle, P. N. Duchesne, R. H. Morris, A. Tavasoli, T. Wood, G. A. Ozin, *Nat. Commun.* **2019**, *10*, 3169.
[16] A. Primo, J. He, B. Jurca, B. Cojocaru, C. Bucur, V. I. Parvulescu, H. Garcia, *Appl. Catal. B* **2019**, *245*, 351–359.
[17] D. Mateo, J. Albero, H. García, *Energy Environ. Sci.* **2017**, *10*, 2392–2400.
[18] F. Sastre, A. V. Puga, L. Liu, A. Corma, H. García, *JACS* **2014**, *136*, 6798–6801.
[19] P. G. O'Brien, A. Sandhel, T. E. Wood, A. A. Jelle, L. B. Hoch, D. D. Perovic, C. A. Mims, G. A. Ozin, *Adv. Sci.* **2014**, *1*, 1400001.
[20] J. Ren, S. Ouyang, H. Xu, X. Meng, T. Wang, D. Wang, J. Ye, *Adv. Energy Mater.* **2017**, *7*, 1601657.
[21] M. Tahir, B. Tahir, N. A. S. Amin, A. Muhammad, *Energy Convers. Manage.* **2016**, *119*, 368–378.
[22] J. Albero, E. Dominguez, A. Corma, H. García, *Sustain. Energy Fuels* **2017**, *1*, 1303–1307.
[23] D. Mateo, D. De Masi, J. Albero, L. M. Lacroix, P. F. Fazzini, B. Chaudret, H. Garcia, *Chemistry* **2018**, *24*, 18436–18443.

[24] R. Grote, R. Habets, J. Rohlfs, F. Sastre, N. Meulendijks, M. Xu, M. Verheijen, K. Elen, A. Hardy, M. van Bael, T. den Hartog, P. Buskens, *ChemCatChem* **2020**, *12*, 5618–5622.
[25] F. Sastre, A. Corma, H. García, *Angew. Chem. Int. Ed.* **2013**, *52*, 12983–12987; *Angew. Chem.* **2013**, *125*, 13221–13225.
[26] F. Sastre, C. Versluis, N. Meulendijks, J. Rodríguez-Fernández, J. Sweelssen, K. Elen, M. K. Van Bael, T. den Hartog, M. A. Verheijen, P. Buskens, *ACS Omega* **2019**, *4*, 7369–7377.
[27] P. G. O'Brien, K. K. Ghuman, A. A. Jelle, A. Sandhel, T. E. Wood, J. Y. Y. Loh, J. Jia, D. Perovic, C. V. Singh, N. P. Kherani, C. A. Mims, G. A. Ozin, *Energy Environ. Sci.* **2018**, *11*, 3443–3451.
[28] X. Yan, W. Sun, L. Fan, P. N. Duchesne, W. Wang, C. Kubel, D. Wang, S. G. H. Kumar, Y. F. Li, A. Tavasoli, T. E. Wood, D. L. H. Hung, L. Wan, L. Wang, R. Song, J. Guo, I. Gourevich, A. A. Jelle, J. Lu, R. Li, B. D. Hatton, G. A. Ozin, *Nat. Commun.* **2019**, *10*, 2608.
[29] D. Mateo, J. Albero, H. García, *Joule* **2019**, *3*, 1949–1962.
[30] J. Barrio, D. Mateo, J. Albero, H. García, M. Shalom, *Adv. Energy Mater.* **2019**, *1902738*, 1902738–1902738.
[31] A. A. Jelle, K. K. Ghuman, P. G. O'Brien, M. Hmadeh, A. Sandhel, D. D. Perovic, C. V. Singh, C. A. Mims, G. A. Ozin, *Adv. Energy Mater.* **2018**, *8*, 1702277.
[32] S. Abate, K. Barbera, E. Giglio, F. Deorsola, S. Bensaid, S. Perathoner, R. Pirone, G. Centi, *Synthesis, Characterization, and Activity Pattern of Ni-Al Hydrotalcite Catalysts in CO2 Methanation, Vol. 55*, **2016**.
[33] H.-K. Wu, F. Zhang, J.-Y. Li, Z.-R. Tang, Y.-J. Xu, *J. Mater. Chem. A* **2020**, *8*, 24253–24266.
[34] V. Dieterich, A. Buttler, A. Hanel, H. Spliethoff, S. Fendt, *Energy Environ. Sci.* **2020**, *13*, 3207–3252.
[35] Y. Wang, Q. Xia, *Chem* **2018**, *4*, 2741–2743.
[36] P. Kaiser, R. B. Unde, C. Kern, A. Jess, *Chem. Ing. Tech.* **2013**, *85*, 489–499.
[37] X. Su, X. Yang, B. Zhao, Y. Huang, *J. Energy Chem.* **2017**, *26*, 854–867.
[38] Y. A. Daza, J. N. Kuhn, *RSC Adv.* **2016**, *6*, 49675–49691.
[39] S. S. Kim, H. H. Lee, S. C. Hong, *Appl. Catal. A* **2012**, *423–424*, 100–107.
[40] B. Dai, G. Zhou, S. Ge, H. Xie, Z. Jiao, G. Zhang, K. Xiong, *The Canadian Journal of Chemical Engineering* **2017**, *95*, 634–642.
[41] X. Li, J. Yu, M. Jaroniec, X. Chen, *Chem. Rev.* **2019**, *119*, 3962–4179.
[42] A. Moores, F. Goettmann, *New J. Chem.* **2006**, *30*, 1121–1132.
[43] A. Gellé, A. Moores, *Curr. Opin. Green Sustain. Chem.* **2019**, *15*, 60–66.
[44] Y. Dubi, Y. Sivan, *Light-Sci. Appl.* **2019**, *8*, 89.
[45] Y. Sivan, I. W. Un, Y. Dubi, *Faraday Discuss.* **2019**, *214*, 215–233.
[46] G. Baffou, R. Quidant, *Chem. Soc. Rev.* **2014**, *43*, 3898–3907.
[47] G. Baffou, I. Bordacchini, A. Baldi, R. Quidant, *Light-Sci. Appl.* **2020**, *9*, 108.
[48] L. Zhou, C. Zhang, M. J. McClain, A. Manjavacas, C. M. Krauter, S. Tian, F. Berg, H. O. Everitt, E. A. Carter, P. Nordlander, N. J. Halas, *Nano Lett.* **2016**, *16*, 1478–1484.
[49] Y. Sivan, J. Baraban, I. W. Un, Y. Dubi, *Science* **2019**, *364*.
[50] L. Zhou, D. F. Swearer, C. Zhang, H. Robatjazi, H. Zhao, L. Henderson, L. Dong, P. Christopher, E. A. Carter, P. Nordlander, N. J. Halas, *Science* **2018**, *362*, 69–72.
[51] Y. Dubi, I. W. Un, Y. Sivan, *Chem. Sci.* **2020**, *11*, 5017–5027.
[52] X. Zhang, X. Li, M. E. Reish, D. Zhang, N. Q. Su, Y. Gutiérrez, F. Moreno, W. Yang, H. O. Everitt, J. Liu, *Nano Lett.* **2018**, *18*, 1714–1723.
[53] Y. Sivan, Y. Dubi, *Appl. Phys. Lett.* **2020**, *117*, 130501.
[54] I.-W. Un, Y. Sivan, *Photothermal effects in plasmonic assisted photocatalysis: a parametric study, Vol. 11694*, SPIE, **2021**.
[55] Y. Sivan, J. H. Baraban, Y. Dubi, *OSA Continuum* **2020**, *3*, 483–497.
[56] R. M. Sarhan, W. Koopman, R. Schuetz, T. Schmid, F. Liebig, J. Koetz, M. Bargheer, *Sci. Rep.* **2019**, *9*, 3060.
[57] R. Kamarudheen, G. J. W. Aalbers, R. F. Hamans, L. P. J. Kamp, A. Baldi, *ACS Energy Lett.* **2020**, *5*, 2605–2613.
[58] I.-W. Un, Y. Sivan, in *OSA Advanced Photonics Congress (AP) 2020 (IPR, NP, NOMA, Networks, PVLED, PSC, SPPCom, SOF)* (Eds.: L. T.-P. A. L. F. Caspani, B. Yang), Optical Society of America, Washington, DC, **2020**, p. NoTh3 C.3.
[59] A. A. Upadhye, I. Ro, X. Zeng, H. J. Kim, I. Tejedor, M. A. Anderson, J. A. Dumesic, G. W. Huber, *Catal. Sci. Technol.* **2015**, *5*, 2590–2601.
[60] B. Tahir, M. Tahir, N. A. S. Amin, *Clean Technol. Environ. Policy* **2016**, *18*, 2147–2160.
[61] M. Tahir, B. Tahir, N. A. S. Amin, Z. Y. Zakaria, *J. CO2 Util.* **2017**, *18*, 250–260.
[62] M. Tahir, B. Tahir, N. A. S. Amin, *Appl. Catal. A* **2017**, *204*, 548–560.
[63] X. Meng, T. Wang, L. Liu, S. Ouyang, P. Li, H. Hu, T. Kako, H. Iwai, A. Tanaka, J. Ye, *Angew. Chem.* **2014**, *126*, 11662–11666; *Angew. Chem. Int. Ed.* **2014**, *53*, 11478–11482.
[64] H. Robatjazi, H. Zhao, D. F. Swearer, N. J. Hogan, L. Zhou, A. Alabastri, M. J. McClain, P. Nordlander, N. J. Halas, *Nat. Commun.* **2017**, *8*, 27.
[65] S. COMSOL Multiphysics(R) v. 5.4. www.comsol.com. COMSOL AB, Sweden.
[66] A. O. Govorov, H. H. Richardson, *Nano Today* **2007**, *2*, 30–38.
[67] G. Baffou, P. Berto, E. Bermudez Urena, R. Quidant, S. Monneret, J. Polleux, H. Rigneault, *ACS Nano* **2013**, *7*, 6478–6488.
[68] I. W. Un, Y. Sivan, *Nanoscale* **2020**, *12*, 17821–17832.
[69] X. Zhang, X. Li, D. Zhang, N. Q. Su, W. Yang, H. O. Everitt, J. Liu, *Nat. Commun.* **2017**, *8*, 14542.

Manuscript received: May 12, 2021
Revised manuscript received: August 16, 2021
Accepted manuscript online: September 3, 2021
Version of record online: September 20, 2021